JOURNAL OF THERMOPHYSICS AND HEAT TRANSFER
Vol. 7, No. 1, Jan.–March 1993

Earth Atmosphere Entry Thermal Protection by Radiation Backscattering Ablating Materials

John T. Howe*
NASA Ames Research Center, Moffett Field, California 94035
and
Lily Yang†
Sterling Software, Palo Alto, California 94303

Hypervelocity entry into Earth's atmosphere can expose the entry vehicle to severe radiative and convective heating environments that can cause ablation and a corresponding transient change in heat shield thickness. A computer code has been developed for a "partially translucent" heat-conducting thermal protection material that backscatters radiation in the depths of the material on a spectral basis, and allows ablation. The code accommodates time-variable finite material thickness, internal material phase change, wavelength-dependent radiative properties, and temperature-dependent thermal, physical, and radiative properties. Various combinations of time-dependent boundary conditions are allowed at both the exposed and backface boundaries. The gas phase of the ablated material from the exposed surface is dynamically mixed with, and thermochemically compatible with, the flowfield, and modifies the time-dependent convective and radiative heating imposed by the energetic airflow. Illustrative examples computed on the Cray 2 are presented. The code is useful to study thermal protection for hypervelocity flight and for material development testing.

Nomenclature

a = inner radius of heat shield shell
$b(t)$ = instantaneous outer radius of heat shield shell
c_p = specific heat of solid
H_s = enthalpy of solid at wall temperature
H_w = enthalpy of gases at surface at wall temperature
h, h' = index on radiation bands that penetrate the heat shield
$I(z, t)$ = radiation intensity
K = Kubelka-Munk radiation absorption coefficient
$\bar{K}$ = radiation absorption coefficient
k = thermal conductivity
m = exponent denoting slab, cylindrical, or spherical coordinates
$\dot{m}(t)$ = mass loss rate by ablation
n = index of refraction
P = directional scattering function
p, p' = index on radiation bands absorbed on exposed surface
$q_r(t)$ = radiative heat flux
$q_w(t)$ = convective heat flux at the wall
r = radius
S = radiation scattering coefficient
$T(z, t)$ = temperature
t = time
$v(t)$ = surface recession rate caused by both ablation and shrinkage
$x(t)$ = distance from exposed surface
$z(t)$ = $x(t)/\delta(t)$
$\delta(t)$ = instantaneous heat shield thickness, $\delta_0 - \int_0^t v(t)\,dt$
μ = cosine of directional angle between radiation intensity and normal to surface
ρ = mass density
ρ = reflectivity

Subscripts
B = pertains to the black body function or Planck's law
c = convection
e = externally incident to heat shield surface
i = internally incident to heat shield exposed surface
o = unblocked flux
o = initial value
R = radiative intensity directed outward in the heat shield
r = radiative
s = internal at backface surface of heat shield
T = radiative intensity directed inward in the heat shield
w = exposed surface (wall) location
ν = spectral radiation band
ν = spectral frequency
∞ = freestream value

Introduction

CONCEPTUALLY, materials which backscatter incident radiative heat fluxes while being simultaneously exposed to convective heating (and are ablating into air) may reduce both the convective and radiative heat load to an entry vehicle significantly. Such a heat shield may be thought of as a "window" for the particular portion of the radiative spectrum to which it is exposed; the significance being that the material does not absorb the radiation excessively. The window material is pulverized to a particle size that backscatters the radiation efficiently. The pulverized material is then reformed into a solid by some process that preserves the granular particulate consistency, which backscatters radiation.

Although the problem of tracing radiative flux in a multiple scattering medium is complicated, the most favorable single

Presented as Paper 91-1321 at the AIAA 26th Thermophysics Conference, Honolulu, HI, June 24–26, 1991; received July 31, 1991; revision received No. 11, 1991; accepted for publication Nov. 13, 1991.

*Chief Scientist. Fellow AIAA.
†Research Specialist, 1121 San Antonio Rd.

particle scattering pattern, has a predominant lobe in the forward (inward) direction for the most efficient overall reflectance of the material.[1] The corresponding particle size is larger than the wavelength of the radiation.[2] It is significant, that the amount of scattering is of more importance than the directional distribution for an individual scattering site for overall "reflection" by the densely packed multiple scattering sites. Thus, the radiation is backscattered in the depths of a weakly absorbing "volume reflector" that does not depend on a smooth mirror surface to reflect the incident radiation. Natural examples of the phenomena are snow and fog, which are translucent or opaque to visible light; each scatters light throughout its volume.

Incident convective heating can also be accommodated simultaneously by the material, even though the combined heating is sufficiently severe to cause surface runoff, ablation, or spallation. Moreover, as the material is heated, the hotter portion may experience a "phase change" wherein the density and thermal properties change, and the material loses its scattering capability (becomes translucent) while the rest of the material still performs as a volume reflector.

The radiative transfer within the material is treated by equations derived from the Schuster equations for radiation in a foggy atmosphere,[3] which are discussed in Refs. 4 and 5. The material response to the combined radiative and convective heating is treated by a transient partial differential equation (energy equation), coupled to the radiative transfer equations. Boundary conditions include transient incident and backscattered radiation, radiation emission, incident convective heating, and ablation of the exposed surface; and any combination of conduction, insulation, reflection, and emission on the rear surface. The ablation is physically and chemically compatible with both the material and the air. The thickness of the material is finite, and varies with time, as it responds to both internal phase change and surface ablation.

The computer program described here incorporates variable material properties in that local thermodynamic, physical, and thermal properties are each functions of temperature. Radiative properties—scattering coefficient, absorption coefficient, and internal radiative emission—are locally functions of wavelength, temperature, and the phase of the material. Therefore, this numerical procedure can be thought of as a benchmark thermal protection material response code. However, refinements can be made, and some will be suggested.

The examples presented illustrate heating environments for hypervelocity flight in air. The authors and their colleagues have previously studied hypervelocity flight in hydrogen-helium atmospheres (for the outer planets) with an earlier code written for another computer, that was less sophisticated, and less user friendly.[6-8] The present code is compatible with both hydrogen-helium and air atmospheres. With suitable detailed input information, it can be used with virtually any combination of materials and atmospheres.

An ablating volume reflector can be one factor in the choice of dimensions for a hypervelocity flight configuration. The convective heating to the stagnation region varies inversely with the square root of the radius, while the radiative heating varies directly with the radius for an isoenergetic shock layer without significant absorption in the gas phase. If the shock layer is nonisoenergetic with gas phase absorption, radiative heating tends to vary directly with the square root of the radius.[9] Conceptually, there exists a surface nose radius that will minimize the combined net convective and radiative heating.

Analysis

Radiative Transfer in the Material

The equation of radiative transfer (of intensity $\bar{I}$ in any (y) direction in a translucent material that emits, scatters, and absorbs radiation of a given wavelength locally is

$$\frac{\mu\, d\bar{I}}{dy}(y, \mu) = -(\bar{K} + \bar{S})\bar{I}(y, \mu) + \frac{\bar{S}}{2}\int_{-1}^{1} P(\mu, \mu')\, d\mu' + \bar{K}n^2\bar{I}_B(y) \tag{1}$$

For isotropic scattering, the scattering function P is unity. The radiative transfer equation can be written in terms of two directional integrated intensities of a given wavelength in the forward and backward directions, respectively, as

$$\frac{1}{2}\left(\frac{dI_T}{d\tau}\right) = -I_T + \frac{\bar{\omega}}{2}(I_T + I_R) + n^2(1 - \bar{\omega})I_B(\tau) \tag{2}$$

$$-\frac{1}{2}\left(\frac{dI_R}{d\tau}\right) = -I_R + \frac{\bar{\omega}}{2}(I_T + I_R) + n^2(1 - \bar{\omega})I_B(\tau) \tag{3}$$

These are the Schuster-Schwarzchild equations,[10] where for the particular wavelength

$$\tau = \int_0^y (\bar{K} + \bar{S})\, dy \tag{4}$$

$$\bar{\omega} = \bar{S}/(\bar{K} + \bar{S}) \tag{5}$$

$$I_T = \int_0^1 \bar{I}(\tau, \mu)\, d\mu \tag{6}$$

$$I_R = \int_{-1}^0 \bar{I}(\tau, \mu)\, d\mu \tag{7}$$

Equations (2) and (3) can be transformed further to obtain the modified Kubelka-Munk equations of bidirectional radiative transfer by the definitions (henceforth, the spectral dependence is explicit and is denoted by the subscript ν)

$$\bar{S} = S_\nu \tag{8}$$

$$\bar{K} = K_\nu/2 \tag{9}$$

which yields

$$\frac{d}{dr}(r^m I_{T_\nu}) = r^m[(S_\nu + K_\nu)I_{T_\nu} - S_\nu I_{R_\nu} - n^2K_\nu I_{B_\nu}] \tag{10}$$

$$\frac{d}{dr}(r^m I_{R_\nu}) = r^m[-(S_\nu + K_\nu)I_{R_\nu} + S_\nu I_{T_\nu} + n^2K_\nu I_{B_\nu}] \tag{11}$$

For $m = n = 0$, these are the Kubelka-Munk equations[11,12] for a slab which absorbs and scatters, but does not emit radiation. Here, radiative emission is included. The coordinate r is measured from the backface of a slab for $m = 0$; or it is the local radius of curvature in a material which has cylindrical or spherical geometry for $m = 1$ or 2, respectively.

Figure 1 shows the geometric and radiative intensity, and flux conventions for an ablating material exposed to radiative and convective heating. The figure pertains to Eqs. (10) and (11) for radiative transfer in a material of original thickness b_o, which diminishes as time progresses. The boundary conditions on the equations of radiative transfer, Eqs. (10) and (11), are

$$(I_{T_\nu})_b = I_{c_\nu}(1 - \rho_{c_\nu}) + \rho_{i_\nu}(I_{R_\nu})_b \tag{12}$$

at the exposed surface, and

$$(I_{R_\nu})_a = \rho_{s_\nu}(I_{T_\nu})_a + (1 - \rho_{s_\nu})I_{B_\nu}(T_a) \tag{13}$$

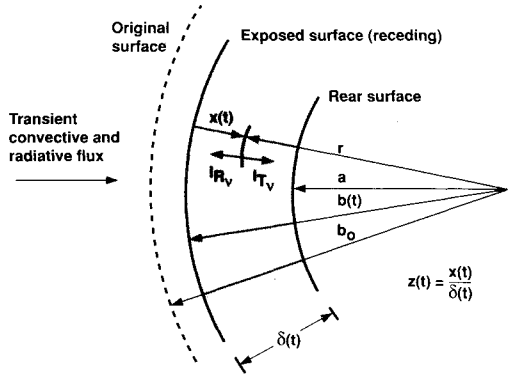

Fig. 1 Coordinate system.

at the rear surface. The factor $(1 - \rho_{s_\nu})$ is the portion of incident radiation absorbed at the surface, which is the same as the surface emissivity.

Energy

The instantaneous energy balance for an element of material located at radius r in the shaded portion of Fig. 1 includes heat conduction; the scattering, absorption, and emission of radiative flux on a spectral basis locally. Geometrically, the instantaneous rate of change of the material thickness includes recession of the exposed surface at the instantaneous velocity $v(t)$ caused by both ablation and densification (phase change). The resulting equation is

$$\rho c_p \frac{\partial T}{\partial t} = \frac{1}{\delta^2 r^m} \frac{\partial}{\partial z}\left(r^m k \frac{\partial T}{\partial z}\right) + \pi \sum_{h}^{h'} K_\nu [I_{R_\nu} + I_{T_\nu} - 2n^2 I_{B_\nu}] + \rho c_p (1 - z) \frac{v}{\delta} \frac{\partial T}{\partial z} \tag{14}$$

The summation is over spectral bands of incident radiation which penetrate the material.

The instantaneous boundary condition at the exposed surface is

$$-\left(\frac{k}{\delta} \frac{\partial T}{\partial z}\right)_0 = \pi \sum_{\nu=p}^{p'} (1 - \rho_{e_\nu})[I_{e_\nu} - I_{B_\nu}(T_w)] + q_w - \dot{m}(H_w - H_s) \tag{15}$$

where the summation is over spectral bands of incident radiation which are absorbed on the exposed surface. At the rear surface, no energy is transmitted from the heat shield material to the aeroshell substrate; i.e., all unreflected radiative flux is absorbed, partially re-emitted, and conducted back into the heat shield material. The interface is insulated to conduction, thus

$$-\left[-\left(\frac{k}{\delta} \frac{\partial T}{\partial z}\right)_{z=1}\right] = \pi \sum_{h}^{h'} (1 - \rho_{s_\nu})[I_{T_\nu}(1, t) - I_{B_\nu}(T_a)] \tag{16}$$

Alternatively, if the substrate is insulated to conduction, but is transparent to radiation, the boundary condition is simply

$$\left(\frac{\partial T}{\partial z}\right)_{z=1} = 0 \tag{17}$$

The initial condition of the heat shield prior to exposure to the heating environment is

$$T(z, 0) = T_o \tag{18}$$

Compatibility of Exposed Surface Material Response to the External Flowfield Environment

At the interface between the thermal protection material and the energetic atmospheric air, several quantities common to each, must be compatible. Our intent is to describe this highly coupled compatibility problem as simply and meaningfully as we can.

The total heat flux from the hot flowfield incident on the wall is composed of convective and radiative components. Without interactive modification it may be written

$$q_{T_o}(t) = q_{w_o} + q_{r_o} \tag{19}$$

These quantities can be obtained from benchmark flowfield solutions, correlations of data or previous solution results, or may simply be specified for parametric studies. They may correspond to test conditions in a ground-based facility or to actual flight.

The net heating at the wall is a modification of these components by factor Ψ. That is

$$q_w = q_{w_o} \Psi_c \tag{20}$$

$$q_{r_\nu} = q_{r\nu_o} \Psi_{r_\nu} \tag{21}$$

where the Ψ functions must be determined. For this paper, Ψ_c and Ψ_{r_ν} are determined from the results of a benchmark flowfield code wherein the gaseous behavior of both the atmosphere and the vaporized material are solved for specified wall temperature, ablation rates, and flight conditions. Solutions are obtained with and without mass addition (or ablation). A set of corresponding values of Ψ_c and Ψ_r are obtained and correlated. Importantly, Ψ_r can be obtained on a spectral basis, Ψ_{r_ν}. The benchmark flowfield code used here is the RASLE code.[13] This code requires a vast amount of input information, and is difficult and costly to use routinely. Therefore, as few benchmark flowfield solutions as reasonable are obtained. The correlation of these results in terms of Ψ_c and Ψ_{r_ν} are used to generalize this information for use in as many flight conditions as desired. The authors are indebted to W. D. Henline[14] for obtaining the present flowfield solutions for SiO_2 ablating into air.

Briefly, by use of information described above and other information described subsequently, a benchmark material solution is obtained. Illustratively, at a given time, flight velocity, surface pressure, flow field enthalpy, and heat fluxes without ablation are known. The state of the material is known at the previous point in time, including material thickness, temperature distribution, mass loss rate, and phase thicknesses (particulate solid or molten). Material properties are known, including density, specific heat, and thermal conductivity as functions of temperature, and optical properties including absorption, scattering and emission coefficients, as well as internal and external surface reflectivities as functions of temperature, wavelength, and material phase.

The solution of the material surface response at the new time is made compatible with the flowfield interface by iteration. Thus, the convective heat blockage factor Ψ_c and the spectral radiative blockage factor Ψ_{r_ν} are obtained from the RASLE solution correlations. The convective blockage function Ψ_c is shown in Fig. 2. The spectral radiative blockage factors Ψ_{r_ν}, obtained from the benchmark flowfield solutions (RASLE), are near unity. Thus, the ablation of SiO_2 into air appears to have little effect on the incident radiation, as shown by the radiative flux spectrum in Fig. 7 of Ref. 14, that will be discussed subsequently. Additionally, an "ablation map" (a set of tables) was obtained a priori by use of flowfield correlations and an equilibrium code "ACE" (Ref. 15) which give thermodynamic and ablation rate information that is self-compatible for chemical equilibrium for the mixture of atmospheric and material gaseous components. Interface in-

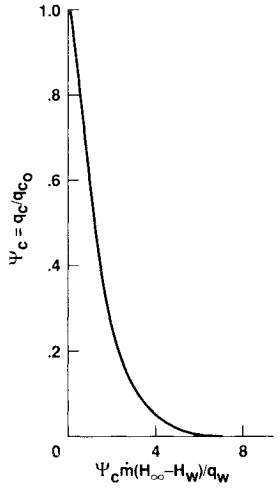

Fig. 2 Convective flux correction: SiO_2 ablating into air.

formation determines the location on that map and provides the ablative boundary condition for the material so that the material energy and radiative transfer equations can be solved iteratively and the solution can be advanced to the next time step. (Ideally, the coupling between the flowfield and the material response should be done by simultaneously solving both benchmark codes. They affect one another simultaneously because the backscattered radiation from the material can alter the flowfield if gas phase absorption is significant.[14,16] Moreover, liquid runoff could be included[17] in completely detailed coupling. This is a major task beyond the resources and scope of the present effort. However, both gaseous interactions and liquid runoff do not appear to be significant in air for the spectral window of SiO_2 and at the high altitudes which will be the emphasis of the examples presented.)

At present, material phase change (melting) and ablation are accounted for. Thus, it is assumed that the material ablates before significant liquid runoff occurs, in accord with the experimental results of Ref. 18 for high altitude aeromaneuvering.

Thermophysical Properties

A very pure silica matrix should be capable of backscattering radiation in approximately the 0.2–2.0 μm spectral range (at least at room temperature). In that spectral range, very pure silica absorbs little radiation. Let us consider a hyperpure silica wherein the particulate material has been slip cast and fused into a solid that backscatters radiation without much absorption, as described by Ref. 19.

The temperature-dependent Kubelka-Munk absorption coefficient input of Fig. 3 corresponds to the 20 spectral bands of radiation input from the flowfield solutions; it was obtained from data in Refs. 20–24 as discussed in Ref. 6.

The scattering coefficient is a function of particle and void size and shape, packing density, and the index of refraction difference between the silica and the voids. Figure 4 shows the Kubelka-Munk scattering coefficient at room temperature for a laminated felt Astroquartz having a fibre size of about 7 μm, a commercial slip cast powdered silica (Glasrock), and hyperpure slip cast fused silica (the material of interest here). The last data were obtained from Ref. 19 and show an improvement in scattering coefficient by a factor of 3 over Glasrock. For present purposes, the scattering coefficient is considered to be invariant with temperature up to the melting temperature (1981 K), at which point it is set to zero. The hyperpure slip cast fused silica scattering coefficient curve will be used in the present study.

The internal exposed surface reflection coefficient of the silica is 0.17 (based on flame glazing tests performed by the first author) for the spectral bands that penetrate the material.

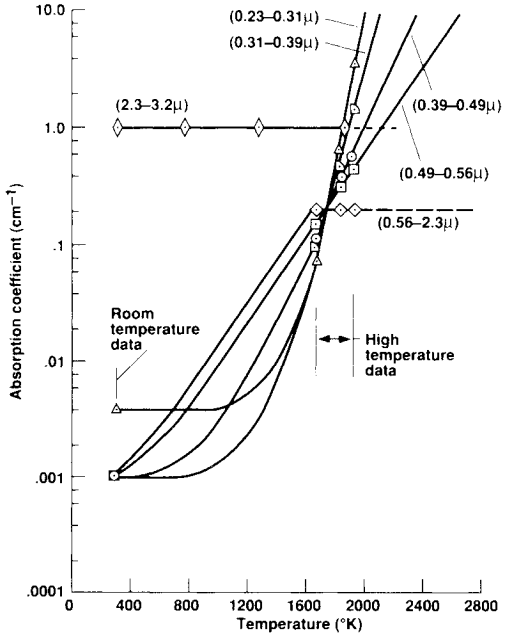

Fig. 3 Temperature-dependent absorption coefficient: "Ultrasil."

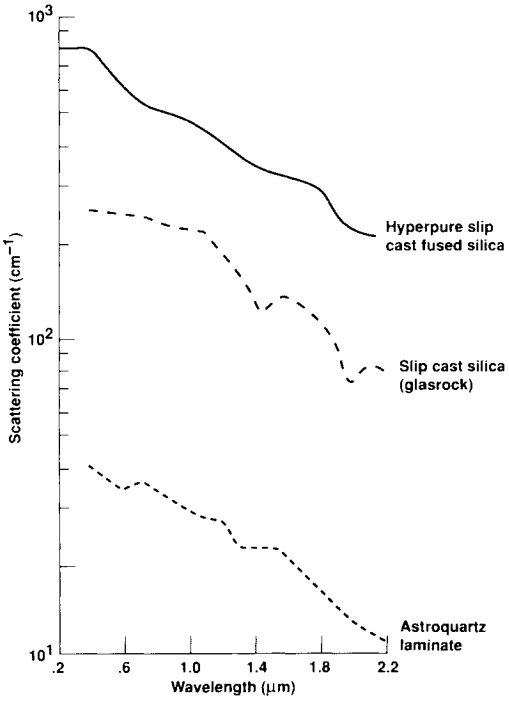

Fig. 4 Spectral scattering coefficient.

The spectral refractive index and its variation with temperature were taken from Ref. 22.

Other properties also vary with temperature. Specific heat varies from about 0.71–1.3 ws/gK from 273 to 1981 K, thermal conductivity (adjusted for density) varies from 0.0088 to 0.023 w/cmK, and density is constant at 1.49 g/cm^3 up to 1981 K (the softening point), at which point the density becomes 2.08 g/cm^3.

A comparison of the properties of silica used here with those of other "window" materials is shown in Table 1, which was obtained from Ref. 25 for room temperature. Thermally the hyperpure slip cast fused silica is a remarkable material; it has a very low thermal diffusivity. It can be shown that compared with ZnSe (which gave the best overall performance for materials exposed to the radiation of Ref. 25) the thermal conductivity of the silica is only 5% of that for ZnSe

Table 1 Thermal properties

Material	Thermal diffusivity, $k/\rho c_p$, cm²/s	Volumetric specific heat, c_p, J/cm³K	Linear absorption coefficient, cm⁻¹
Ionic bond			
KBr	0.040	1.2	0.00005
Covalent bond			
CdTe	0.049	1.23	0.002
ZnSe	0.096	1.87	0.005
CdS	0.148	1.82	0.03
GaAs	0.338	1.42	0.02
Ge	0.358	1.65	0.032
SiO_2	0.0054	1.63	0.001–0.004

at room temperature. The linear absorption coefficients are comparable.

Illustrative Results

First, results of an example of entry of a vehicle with a backscattering heat shield entering the atmosphere of Earth upon returning from Mars is presented. The entry is very energetic (14 km/s), and vehicle (shown in the inset of Fig. 5) flies a 5g limited undershoot trajectory obtained from Ref. 26.

Figure 5 was adapted from Ref. 14, obtained from RASLE benchmark flowfield solutions, with and without SiO_2 ablation. It shows the spectral radiative flux incident upon the heat shield. Two features are significant for present purposes; first, the SiO_2 ablation products have little effect on the incident radiation (Ψ_{r_w} is near unity) for wavelengths of radiation which penetrate the heatshield (from about 0.2–2.0 μm). Second, a large part of the incident spectrum is in the ultraviolet which is partially absorbed and reflected from the surface of the heat shield. This is about half of the incident radiative flux.

The actual heating pulse is shown in Fig. 6. In accord with Ref. 14, the convective heating pulse and the radiative heating pulse (reduced by 45%) obtained from Ref. 26 were used. It is significant that the heating rate is dominated by a long convective pulse and includes a relatively short radiative pulse. In this example, about half the radiative heating is absorbed on the exposed surface, in addition to the convective heating that reaches the surface. The other half of the radiation penetrates the material. Because of the long duration of heating, thermal soak is important. It may be noted, that none of the heat that is radiated or conducted to the rearface of the material, passes through that surface because of the boundary condition expressed by Eq. (16).

Figure 7 shows the exposed and rear surface temperature history computed by the code. The peak exposed surface temperature is below 3000 K and occurs at the point of peak heating. At the end of the radiative heating (at about 190 s), the exposed surface temperature momentarily increases slightly, corresponding to the slight change in the ablation rate.

At the end of the long heating pulse (500 s) the rearface temperature is about 500 K. For an allowable rearface temperature of 700 K, the corresponding heat shield thickness could be about 5.6 cm. The original density of the slipcast fused silica heat shield is about 1.5 g/cm³. Thus, the weight of the heatshield material (exclusive of insulation, although there is an insulation option that has not been exercised) is about 8.4 g/cm², or 17 lbm/ft². This value is above that for insulated carbon phenolic (9.66 lbm/ft²) and near that for carbon carbon (17.25 lbm/ft²) shown in Table 4 of Ref. 14 for this application. Thus, this material is not particularly well suited for this entry dominated by a long convective heating pulse. The material does have the attribute that without heat loss through the rearface, the temperature there is moderate. More importantly, the example illustrates that the present

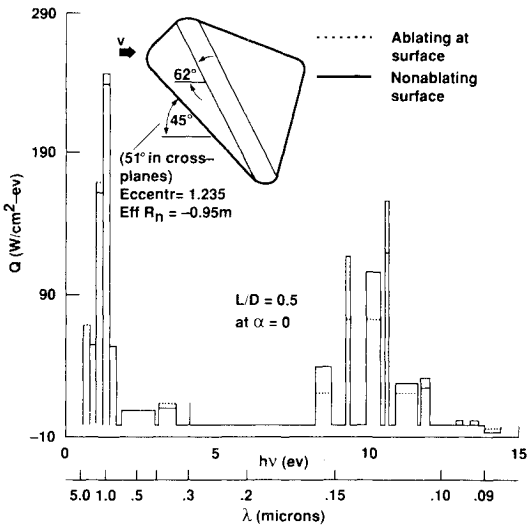

Fig. 5 Spectral line radiative fluxes; Mars return, SiO_2 in air (adapted from Ref. 14).

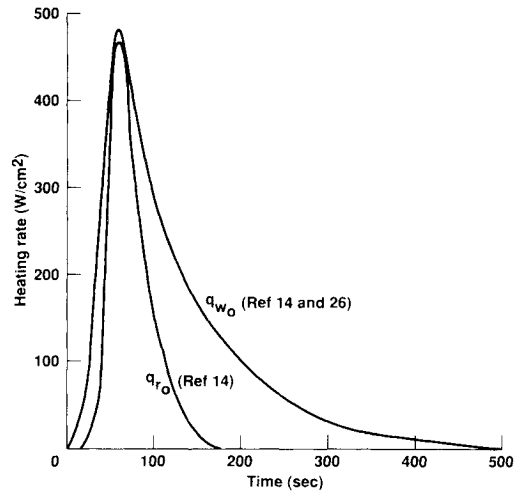

Fig. 6 Heating rate history manned Mars return.

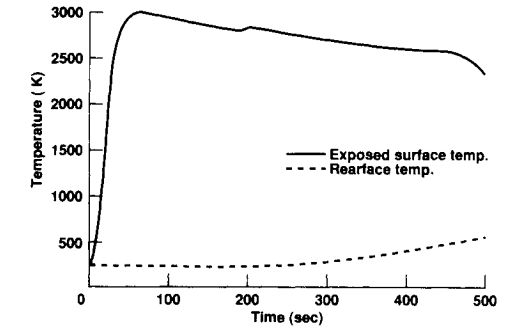

Fig. 7 Transient boundary temperatures shown on a backscattering silica heat shield with an initial thickness of 6 cm. Material response in air for 14 km/s entry into Earth atmosphere.

computer code is a useful tool for the development of a more suitable material which backscatters radiation over a broader radiative spectrum, has desirable thermal properties and ablative properties, and can predict the material performance in this or any other application.

The internal temperature profiles of the heat shield at various moments in time is shown in Fig. 8. It may be noted that at the end of the radiative heat pulse (190 s), about 87% of the remaining heat shield is under 2000 K, has not melted, and is still able to backscatter radiation.

Finally, the total surface recession history caused by ablation is shown in Fig. 9. Altogether, the heatshield receded

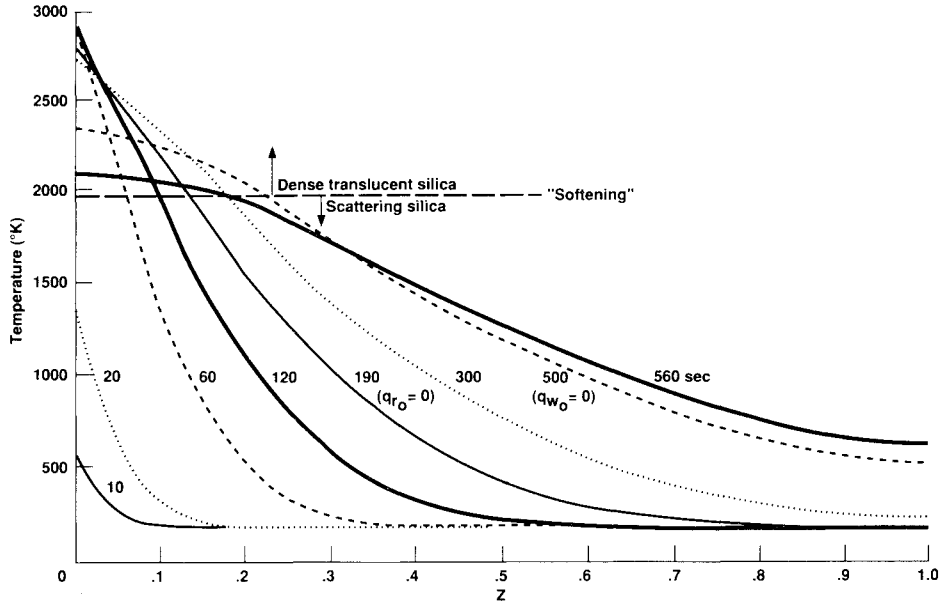

Fig. 8 Transient internal temperature profiles, the initial thickness is 6 cm.

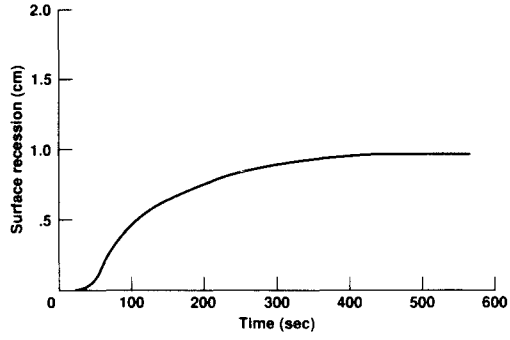

Fig. 9 Surface recession due to mass loss, the initial thickness is 6 cm.

about 0.95 cm. This can be compared with the results shown in Fig. 13 of Ref. 14 for the same environment. As expected, it is significantly larger than the recession of carbonaceous materials, but is less than that of Avcoat (about 2 cm) and RSI (LI-2200), which is about 4.3 cm. Thus, the ablation loss ratio (0.95 cm/4.3 cm = 0.22) is comparable to the inverse density ratio, (22 lbm/ft^3)/(93 lbm/ft^3) = 0.24, which indicates that the total mass loss per surface area is about the same for slip cast fused silica and RSI (an interesting result, that is to be considered illustrative only).

In order to further demonstrate some features of the material response code, we now specify a heating history shown in Fig. 10. The intent is to contrast the heat shield material response to combined convective and (dominantly) radiative heating with convective heating only. The specified heating rate history (Fig. 10) is a sinusoidal heat pulse lasting 150 s wherein the peak radiation is 1000 w/cm^2 and peak convection is 200 w/cm^2. This may be thought of as representing a model in a test facility where test conditions can be specified. This convenience allows us to use the voluminous input information that exists for SiO_2 in air. This information includes all material thermal, physical, and spectral optical properties (and their variation with temperature), incident convective and spectral radiative blockage caused by ablation, the SiO_2/air ablation map, and our prior pressure and enthalpy history.

For a heat shield model that is initially 4-cm thick, that does not lose any heat out the rearface [boundary condition Eq. (16)], the surface temperature histories are shown in Fig. 11. As expected, the exposed surface temperature for combined radiative and convective heating exceeds that for convection alone. The heat shield begins to ablate significantly

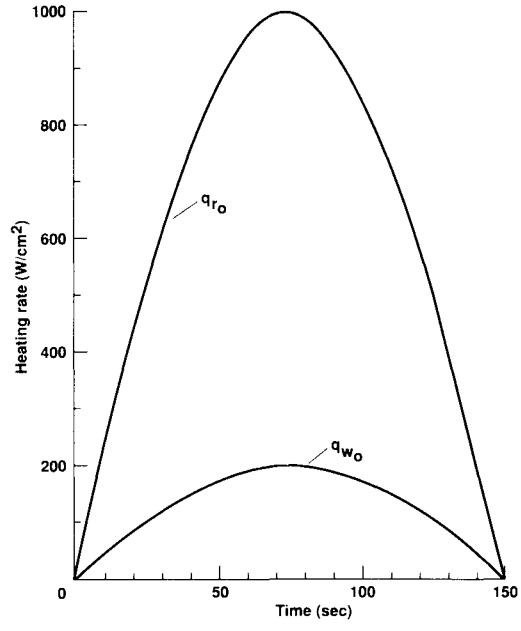

Fig. 10 Illustrative heating rate history that is radiation dominated.

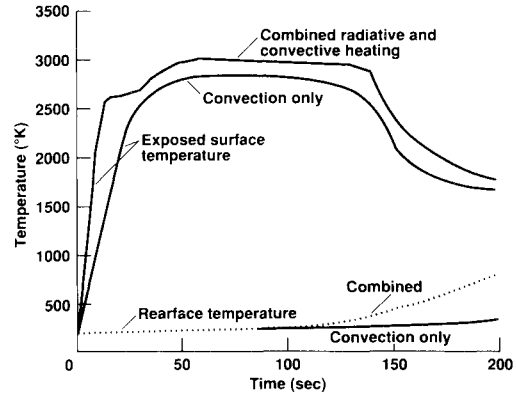

Fig. 11 Transient boundary temperatures shown in a backscattering silica heat shield with an initial thickness of 4 cm; material response in air.

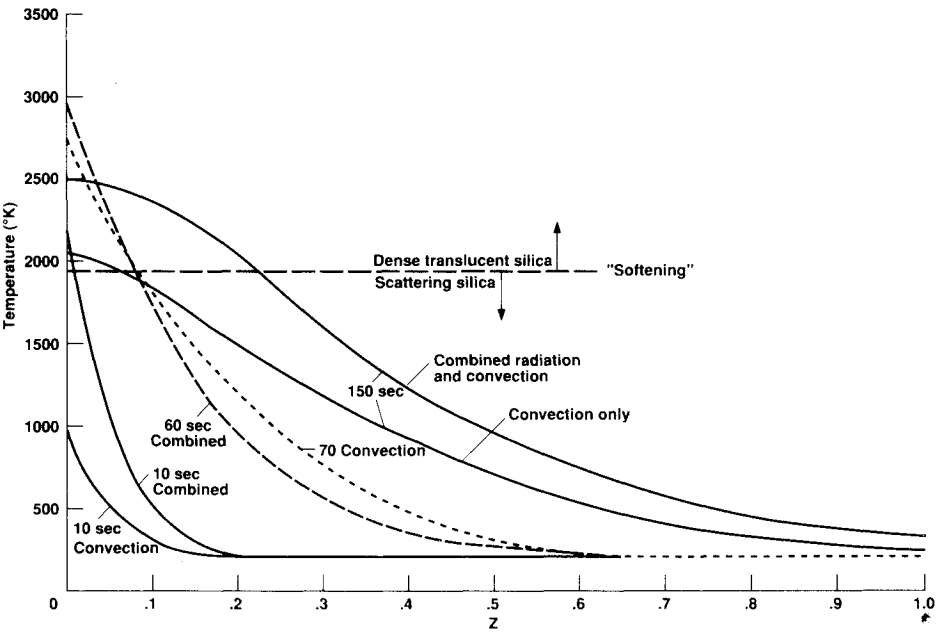

Fig. 12 Transient internal temperature profiles with an initial thickness of 4 cm.

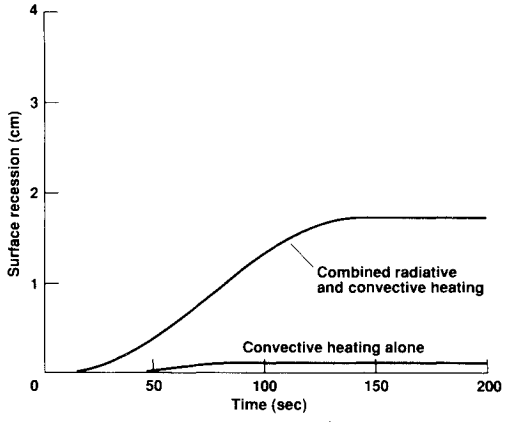

Fig. 13 Surface recession due to mass loss with an initial thickness of 4 cm.

at about 15 s for combined heating, that results in a sharp break in the slope of the surface temperature. At about 145 s, the combined heating rate has dropped so that ablation cannot be sustained and the exposed surface temperature drops sharply. Incidentally, both of these points correspond to the surface recession plot, which will be discussed subsequently. The combined heating pulse ends at 150 s.

The rearface temperature history shown in Fig. 11 for combined heating is about 400 K at 150 s. A common allowable interface temperature is 700 K, so that the heat shield could have been less than 4-cm thick initially.

Figure 12 shows temperature profiles for combined heating and for convective heating alone at various moments in time. Just below 2000 K, the material softens, experiences an increase in density, a corresponding shrinkage, a change in thermal properties, and absorbs (but does not backscatter) radiation. Thus, a "front" moves through the material as it heats internally, behind which the material properties change. At peak heating (75 s), about 90% of the remaining material has not softened or melted and continues to backscatter radiation.

The surface recession caused by ablation (exclusive of shrinkage) is shown as a function of time in Fig. 13. For combined heating, the original 4-cm thick heat shield has lost about 1.75 cm by ablation at the end of the heating. In contrast, recession caused by convection alone is only about 0.065 cm, mostly because of the effectiveness of blockage by ablation (Fig. 2). The overwhelming cause of ablation is unblocked radiation in accord with Ref. 27, wherein heating was doubled by adding an equal unblocked radiative component to the convective heating, that caused a sixfold increase in ablation rate.

Concluding Remarks

A heat shield material response code has been written that predicts the transient performance of the material subject to the combined convective and radiative heating associated with hypervelocity flight. The code is dynamically interactive to the heating from a transient flow field, including the effects of material ablation on flowfield behavior. The code treats the effects of surface heating by convection and radiation, and the simultaneous internal response to radiation, which penetrates the depths of the material. Physical and thermal properties of the material are temperature dependent, while radiative properties at both the surface and in the depths of the material, are both temperature and spectrally dependent. That portion of the incident radiation which penetrates the material is partially absorbed, scattered, and re-emitted in depth, and includes the effects of partial internal reflections and/or transmission at the boundaries of the material. The thickness of the heat shield is a self-determined function of time as the heat shield ablates in response to heating by the flowfield. Computationally, the equations of radiative transfer are solved within the material, and are coupled to the transient energy equation that contains the radiative flux divergence in addition to the usual energy terms.

Illustrative results are presented from solutions of the coupled equations for silica heat shields in air, for both convection dominated and radiation dominated combined heating. For the latter situation, it was shown that for weak flowfield blockage of incident radiation, the resulting large ablation rates induced by radiation effectively block the convective heating.

The code includes such an abundance of flowfield and material property detail, that it should be useful for the study of thermal protection problems for hypervelocity flight in the atmosphere, and the development of specialized thermal protection materials in the laboratory.

References

[1]Ross, W. D., "Theoretical Computation of Light Scattering Power," *Journal of Paint Technology*, Vol. 43, No. 563, 1971, pp. 50–66.

[2]Brumberger, H., Stein, R. S., and Powell, R., "Light Scattering," *Science and Technology*, Vol. 1, Nov. 1968, pp. 34–42.

[3]Schuster, A., "Radiation Through a Foggy Atmosphere," *Astrophysics Journal*, Vol. 21, No. 1, 1905, pp. 1–22.

[4]Viskanta, R., "Radiation Transfer and Interaction of Convection with Radiation Heat Transfer," *Advances in Heat Transfer*, Vol. 3, Academic Press, New York, 1966, pp. 176–251.

[5]Chandrasekhar, S., *Radiative Transfer*, Dover, New York, 1960, Chap. 1.

[6]Howe, J. T., and McCully, L. D., "Volume Reflecting Heat Shields for Entry into the Giant Planet Atmospheres," *Heat Transfer with Thermal Control Applications*, edited by M. M. Yovanovich, Vol. 39, Progress in Astronautics and Aeronautics, 1975, pp. 349–371.

[7]Liu, C. H., and Howe, J. T., "Entry into the Outer Planet Environments: Part 1, The Radiating Shock Layer with Coupled Ablation for Carbon and Silica," *Thermophysics of Spacecraft and Outer Planet Entry Probes*, edited by A. M. Smith, Vol. 56, Progress in Astronautics and Aeronautics, MIT Press, 1977, pp. 291–305.

[8]Howe, J. T., "Entry into Outer Planet Environments; Part 2, Performance of Volume Reflecting Hyperpure Silica Heat Shields," edited by A. M. Smith, Vol. 56, *Thermophysics of Spacecraft and Outer Planet Entry Probes*, Progress in Astronautics and Aeronautics, MIT Press, 1977.

[9]Howe, J. T., and Viegas, J. R., "Solutions of the Ionized Radiating Shock Layer Including Reabsorption and Foreign Species Effects and Stagnation Region Heat Transfer," NASA TR-R159, 1963.

[10]Hottel, H. C., and Sarofim, A. F., Radiative Transfer, McGraw-Hill, New York, 1967, p. 430.

[11]Kubelka, P., and Munk, R., "Ein Beitraq zur Optik der Farbenstriche," *Zeitschrift für Technische Physik*, Vol. 12, 1931, p. 593.

[12]Steele, F. A., "The Optical Characteristics of Paper," *Paper Trade Journal*, March 1935, pp. 151–156.

[13]Nicolet, W. E., and Balakrishnan, A., "Radiating Shock Layer Environment, RASLE," (User's Manual), Acurex Rept. UM-79-10/AS, July 1979.

[14]Henline, W. D., "Aerothermodynamic Heating Environment and Thermal Protection Materials Comparison for Manned Mars-Earth Return Vehicles," AIAA Paper 91-0697, Reno, NV, 1991.

[15]Anon., Aerotherm Chemical Equilibrium Computer Program (ACE81), Acurex Rept. UM-81-11/ATD, Aug. 1981.

[16]Howe, J. T., "Shielding of Partially Reflecting Stagnation Surfaces Against Radiation by Transpiration of an Absorbing Gas, NASA TR R-95, 1961.

[17]Hidalgo, H., "Ablation of Glassy Material Around Blunt Bodies of Revolution," *American Rocket Society Journal*, Vol. 30, No. 9, 1960, pp. 806–814.

[18]Henline, W. D., Tran, H. K., and Hamm, M. K., "Phenomenological and Experimental Study of the Thermal Response of Low Density Silica Ablators to High Enthalpy Plasma Flows," AIAA Paper 91-1324, Honolulu, HI, June 1991.

[19]Blome, J. C., Drennan, D. N., and Schmitt, R. T., "High Purity Silica Reflective Heat Shield Development," NASA CR-137617, Oct. 1974.

[20]Rupp, R. L., "High Temperature Transmission Studies of Window Materials for Project Fire," NASA Scientific and Technical Information Facility, Doc. N6586594, Aug. 1965.

[21]Luckey, D. A., "Optical Properties of Fused Quartz for Project Fire Radiometer Data Analysis," NASA Flight Reentry Programs Office, Working Paper 24, Oct. 1963.

[22]Anon., *Optical Fused Quartz Fused Silica*, Amersil Inc., Hillsdale, NJ, 1971.

[23]Beder, E. C., Bass, C. D., and Shackleford, W. L., "Transmissivity and Absorption of Fused Quartz Between 0.22 and 3.5 μm from Room Temperature to 1500°C," *Applied Optics*, Vol. 10, No. 10, 1971, pp. 2263–2268.

[24]Spivak, J. F., "High Temperature Infrared Transmission Studies of Ultraviolet Fused Quartz for Project Fire," Republic Aviation Corp., RZC499-38 (RD-TR-64-637), June 1964.

[25]Howe, J. T., "Volume Reflecting Coating for Laser Hardening," NASA TMX-3506, 1977, Declassified Dec. 31, 1982.

[26]Tauber, M. E., Palmer, G. E., and Yang, L., "Earth Atmospheric Entry Studies for Manned Mars Missions," AIAA/ASME Joint Thermophysics and Heat Transfer Conference, AIAA Paper 90-1699, Seattle, WA, 1990.

[27]Bartlett, E. P., Nicolet, W. E., and Howe, J. T., "Heat-Shield Ablation at Superorbital Re-Entry Velocities," *Journal of Spacecraft and Rockets*, Vol. 8, No. 5, 1971, pp. 456–463.